Journal of Sound and Vibration (1998) **213**(4), 577–600

INVESTIGATIONS OF LOW FREQUENCY STICK–SLIP MOTION: EXPERIMENTS AND NUMERICAL MODELLING

V. G. Oancea and T. A. Laursen

Department of Civil and Environmental Engineering, *Box* 90287, *Duke University*, *Durham*, *NC* 27708-0287, *U.S.A.*

(*Received* 10 *July* 1996, *and in final form* 22 *December* 1997)

Dry frictional contact between two steel surfaces in a harmonically forced spring–mass system is investigated both experimentally and numerically. The experimental set-up is somewhat novel in that the spring–mass system is excited through the frictional interface, facilitating detailed study of interactions between the system's dynamic characteristics and the stick–slip motion observed at the interface. A characterization of the effect of wear upon observed stick–slip is given, resulting in the identification of three sliding regimes displaying varying degrees of wear. Subsequent attention is focused primarily on the first of these regimes, the low wear regime, which features low frequency stick–slip oscillations that can be measured quite reliably. This work particularly emphasizes the nature of transients entering and exiting stick phases, with several representations given of the evolution of these transients as control parameters are changed. Multiperiod and chaotic motions of the mass are also observed, with routes to chaos being qualitatively similar for a wide range of system parameters. The work also presents some numerical results in support of the experimental work, utilizing a rate- and state-dependent friction model proposed previously by the authors. It is seen that this model yields significantly better predictions than can a simple Coulomb representation.

1. INTRODUCTION

This work concentrates on the issue of friction induced vibration. Of particular interest is stick–slip motion, which often takes the form of self-sustained oscillation induced by dry friction. A number of attempts may be found in the literature to experimentally study the dynamics of such systems. A sampling of these works also provides a useful survey of the applications of such work. Bell and Buderkin [1] report an extensive study of stick–slip oscillations of the feed drives of machine tools, and outline the factors contributing to this type of instability. Other authors studied the dynamics of frictional systems for specific applications like squeal noise of wheel–rail systems (e.g., Fingberg [2]) or whirl motion of drillstrings (e.g., Van der Heijden [3]). Other experiments of a less applied nature have investigated the effects of system stiffness on friction, wear, and vibrations [4], the relationship of stick–slip behaviour to normal high frequency vibrations [5–7], and the relationship between stick–slip vibrations and chaos (e.g., references [8–10]).

In this work, a harmonically forced linear spring–mass system under constant normal load is studied, with the only significant non-linearity emanating from a frictional interface through which the forcing occurs. For different choices of control parameters (stiffness, normal force, amplitude and frequency of the forcing) the periodicity of stick–slip oscillations can be readily monitored. Also, the transients entering and exiting periods of

0022–460X/98/240577 + 24 $25.00/0/sv971496

stick are investigated. Several sliding regimes are identified as a function of total sliding distance, with attention being focused primarily in this work on a regime characterized by low to moderate surface damage and low frequency stick–slip motion.

This experimental effort is accompanied by some numerical simulations using a phenomenological rate- and state-dependent friction model proposed by the authors in a previous work [11]. The friction law is written in terms of variables defined pointwise on the interface, and is mechanically coupled to its surroundings through the slip displacement, the normal interface stresses, and the tangential stresses. It features a state variable approach [12] for description of long-term effects and a viscoplastic regularization [13] for highly transient phenomena. General experimental observations about stick–slip motion are verified, including decrease of stick–slip amplitude as driving velocity increases, spring stiffness increases, or mass decreases. It will be shown that the state variable model can predict multi-periodicity and chaos as observed in experiment where a simpler Coulomb description cannot.

The outline of the paper is as follows. In section 2, the experimental set-up is briefly presented. Results obtained from this experimental apparatus are presented in section 3, while section 4 gives a brief review of the friction model used in the numerical study as well as a summary of the numerical results obtained using it. Finally, some concluding remarks are given in section 5.

2. EXPERIMENTAL SET-UP AND PROCEDURE

A schematic of the apparatus used in the experiment is shown in Figure 1. Two identical horizontal spring steel beams, referred to as the main beams, are cantilevered between the rigid blocks and support the masses, accelerometers, and the beams 1 and 2 as shown in the figure. A steel sphere mounted at the end of the vertical beam 2 is sliding with dry friction over the friction plate, which is itself attached to the linear slide. This slide is

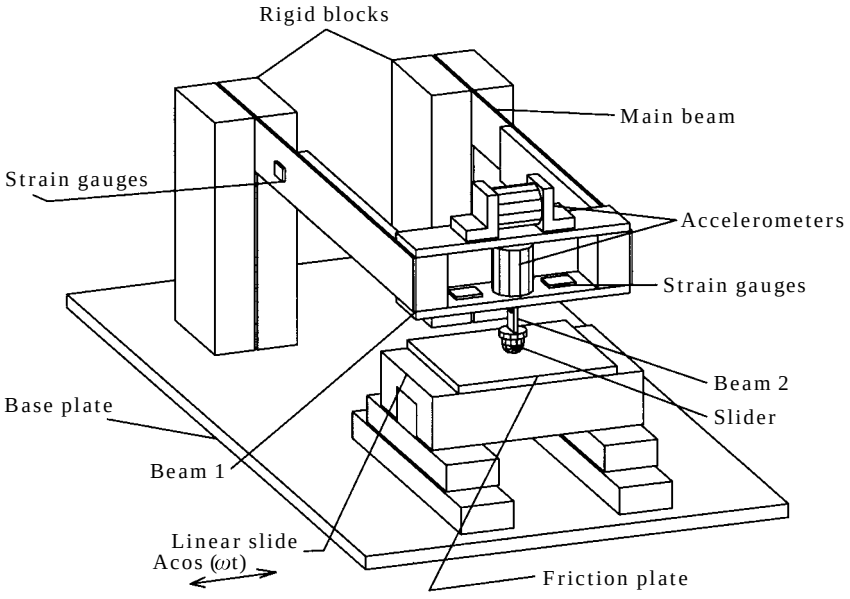

Figure 1. Schematic of test apparatus.

excited harmonically by an electromagnetic shaker, so that friction between the steel plate and the sphere induces lateral motion of the cantilevered mass.

The main beams are 25 mm wide and 0·5 mm thick, and their length can be altered between 160 and 300 mm by changing the clamping position between the rigid blocks. Constrained layer damping using stiff aluminum plates taped to the beam is employed, such that the higher modes of vibration of these beams are damped. The distance between the spring beams is 105 mm, and was chosen so that the amount of rotation of the mass about an axis parallel to the main beams is negligible. The base plate incorporates an adjustable clamping system (not shown) such that by slight bending of the base plate (8 mm thick) the normal load on the steel plate can be altered in a continuous manner.

The measuring system consists of three strain gauge bridges, two accelerometers and one LVDT. A half-bridge attached to one of the main beams is used to measure displacements of the contact point of the sphere. A full bridge mounted on beam 1 and a half bridge on beam 2 are used to measure normal and frictional interface forces, respectively. The first mode of beam 1 was found to be at 457 Hz while the second mode was estimated to be at 1326 Hz. For beam 2 the first two natural frequencies were 562 and 2605 Hz. Two piezoelectric accelerometers are used to measure normal and tangential accelerations of the mass, while an LVDT (not shown) monitors the displacements of the linear slide. The suspended mass including all instrumentation, wires, and aluminum stiffeners is 530 g.

The analogue voltage output signals were fed into appropriate signal conditioners and amplifiers, and then given as input to an analogue/digital data acquisition package on a personal computer. The data were then digitally filtered, using bandstop filter data for 60 Hz and in most cases further filtering with a cut-off frequency of 100 Hz.

Calibrations for all strain gauge bridges and for the LVDT were done *in situ* using the data acquisition package described above, while the displacements of the linear slide were calibrated using a dial gauge. In order to make an accurate calibration for the relative displacements between the linear slide and the sphere contact tip, the head displacements were calibrated by imposing perfect stick at all times so that the displacement of the sphere tip was the same as that of the stage. The scaling between the voltage from the gauges on the main beam and the linear slide displacements was then determined, allowing the accuracy of relative positioning measurements to be increased up to the noise level of the measuring system (about 10 μm). The sensitivity of the normal and friction force measuring systems were 0·1 and 0·05 N, respectively.

Experiments were conducted with steel on steel as friction materials. For the steel plate a spring steel hardened at 56 Rockwell C was used, while a ball bearing (69 Rockwell C) was used as the pin material. No lubrication was used at any time and the samples were carefully cleaned with alcohol before each experiment. Ambient temperature was found to vary between 18 and 23°C.

3. EXPERIMENTAL RESULTS

Four control parameters are of particular interest in the results that follow: amplitude A (0·5–9 mm) and frequency f (3–10 Hz) of the excitation provided to the linear slide, normal force t_N (2–15 N) existing across the frictional interface, and the collective stiffness k of the two main beams (250–18 000 N/m). The results are organized under three primary headings: (1) an assessment of the effect of wear on the dynamics of sliding; (2) a characterization of the transients observed during stick–slip cycles; and (3) a study of the periodicity of low frequency stick–slip behaviour, exhibiting in particular multiperiod and chaotic features.

3.1. SLIDING REGIMES

Wear is potentially a significant feature of this experiment, given the repetitive nature of the interface loading. An important first step was thus to investigate the effect of prolonged sliding on system dynamics. In all experiments the normal load was kept sufficiently low so that wear rates on the sphere were insignificant, making the wear on the comparatively soft steel plate the phenomenon of interest. Preliminary tests showed that wear conditions and resulting dynamics could vary widely from test to test during the first hour or so of testing after beginning with fresh sliding surfaces. Accordingly, to standardize the testing procedure, a "wearing in" period was employed at the beginning of each test, whereby the normal load was set to $t_N = 3{\cdot}0$ N and the system was allowed to oscillate for a period of at least 1 h at the forcing amplitude A and frequency f of interest. After this time the normal force was set to the desired value and data collection commenced. A number of experiments were performed, employing various combinations of control parameters and lasting between 6 and 12 h. Invariably, three sliding regimes were found to characterize the dynamics of the system in time. An overview of these three sliding regimes follows, as obtained for the following parameter combination: $A = 8$ mm, $f = 3$ Hz, $t_N = 4{\cdot}2$ N and $k = 853$ N/m.

3.1.1. *Low frequency vibration regime*

The first sliding regime is characterized by virtually no induced acceleration normal to the interface, indicating that sliding occurs rather smoothly (i.e., without inducing jumping behaviour in the normal direction). Stick–slip behaviour does occur, however, with the tangential acceleration and traction displaying noticeable low frequency oscillations in a manner suggestive of a history dependent response. Figure 2(a) shows the normalized tangential and normal accelerations versus time over three cycles after the limit cycle is reached. The oscillations of the mass are seen to be quite similar (but not identical) for both directions of the slide stroke, with the slight asymmetry believed to be caused by different out of stick transients induced at the two stage reversals occurring in each cycle.

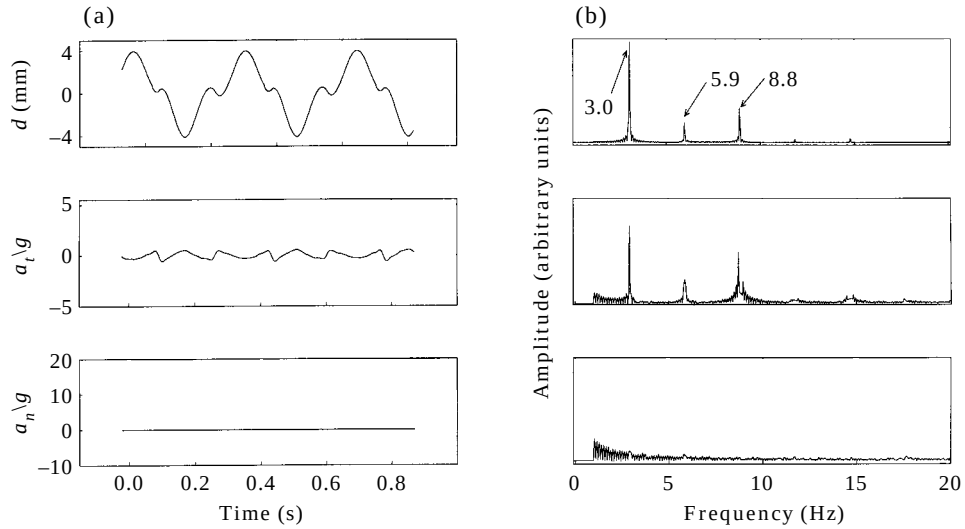

Figure 2. Smooth sliding regime: (a) experimental sphere tip displacements (d), tangential (a_t) and normal (a_n) accelerations shown for three forcing cycles (filtered using 100 Hz cut-off frequency); (b) corresponding power spectra for the time series shown in (a) bandstop filtered at 60 Hz only (sampling frequency = 1 kHz).

The power spectra shown in Figure 2(b) show that insignificant energy is to be found in the high frequency range, and also verify the lack of normal acceleration mentioned above. The three-period motion of the main beam involves the three frequencies apparent from the figure: 3·0 Hz is the forcing frequency, while the other two frequencies are close to the natural frequency of the beam (estimated as 6·5 Hz in a separate test). If the 5·9 Hz frequency can be interpreted as the frequency of the friction damped system, the 8·8 Hz frequency is more difficult to explain. Another possible explanation is that the observed spikes are subharmonic resonances.

The duration of this low frequency vibration regime was approximately 5 h for this combination of control parameters. A metallographic photo of the plate after 2 h of sliding is shown in Figure 3(a). The black spots are the hills of the asperities while the whiter spots are the valleys. The surface appears only slightly damaged when compared to an initial sample (not shown). Also, the in-plane average size of the asperities is quite large (25 μm).

3.1.2. *High frequency vibration regime*

After approximately 5 h of sliding, the onset of the second sliding regime was detectable through a slight increase of the peak friction force observed at stage direction reversal. Subsequently, the higher modes of beams 1 and 2 were sporadically excited, causing the measurements of normal and friction force to be meaningless. However, the accelerometers have a much higher resonant frequency and their measurements are shown in Figure 4(a). As can be seen, the asymmetries in tangential slider displacement are more accentuated than in the first regime, and the high frequency modes become excited in short bursts immediately prior to direction reversal of the stage in each cycle. The frequency spectra for the tangential displacement and acceleration show peaks at low frequencies (3·0 and 5·9 Hz) as in the first sliding regime, while the peak at 8·8 Hz is no longer observed. Both spectra show a peak fiin the vicinity of 562 Hz, which is thought to correspond to the first natural frequency of beam 2. The other high frequency peaks correspond to the higher modes of vibration of beams 1 and 2.

Interestingly, the low frequencies apparent in the tangential acceleration spectra are not seen in the normal acceleration, with any coupling between the frictional and normal degrees of freedom seemingly occurring only for higher frequency oscillations. The occurrence of low frequency oscillation only in the frictional direction is qualitatively similar to the observations in Aronov *et al*. [4] for constant velocity sliding. This second sliding regime lasted for about 2 h. A metallographic picture of the surface after 6 total hours

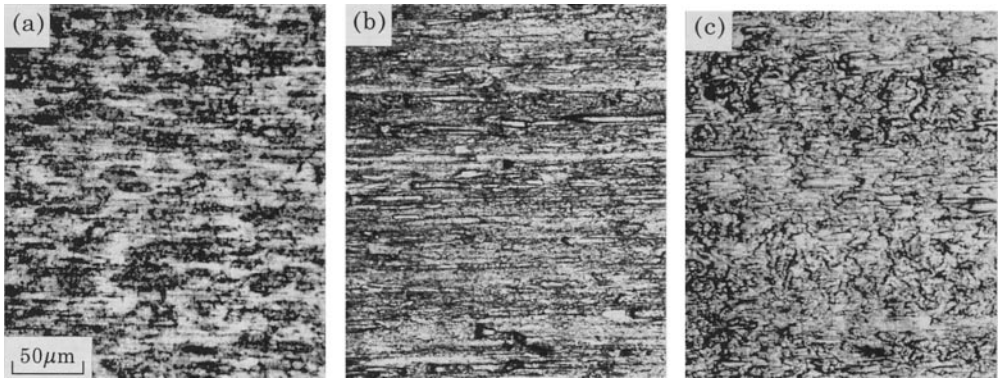

Figure 3. Evolution of surface asperity appearance versus sliding time: (a) after 2 h of sliding; (b) after 6 h of sliding; (c) after 8 h of sliding. Sliding times measured after the running-in period.

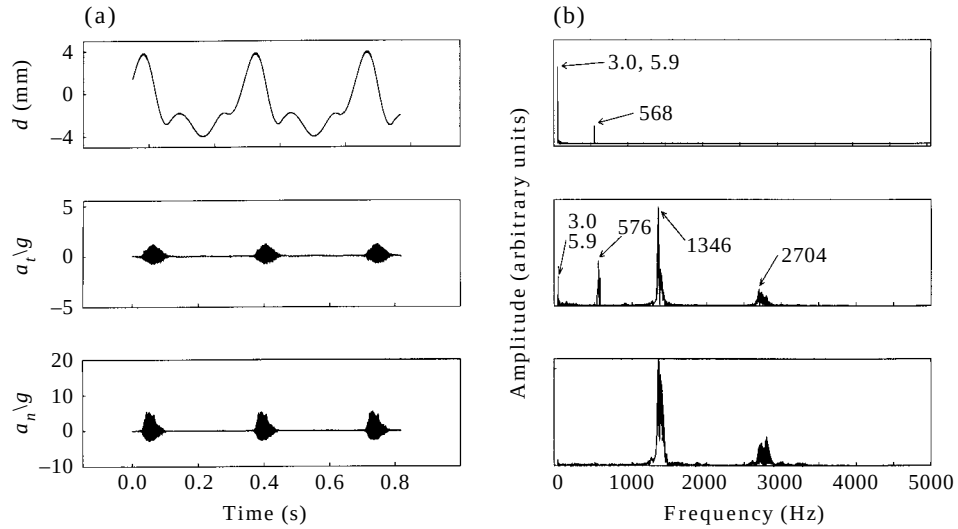

Figure 4. High frequency vibration regime: (a) experimental sphere tip displacements (d), tangential (a_t) and normal (a_n) accelerations shown for three forcing cycles; (b) corresponding power spectra (sampling frequency = 10 Hz).

of sliding (after the running-in period) is shown in Figure 3(b). Comparison with Figure 3(a) verifies that the wear process is no longer mild and that the in-plane average asperity size is reduced (10 μm).

3.1.3. *Severe wear sliding regime*

About 7 h after the running-in period, much stronger high frequency vibrations appear sporadically during sliding in both directions. The asymmetries of the mass displacement become even stronger (Figure 5(a)), with a slight increase in amplitude. A periodic pattern can be seen where high frequency vibrations occur in both directions of sliding. The

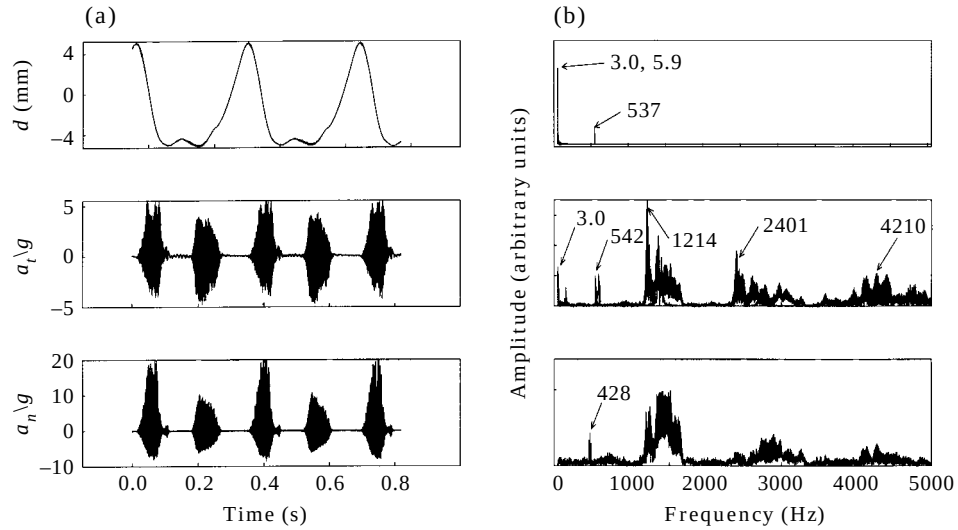

Figure 5. Severe wear sliding regime: (a) experimental sphere tip displacements (d), tangential (a_t) and normal (a_n) accelerations shown for three forcing cycles; (b) corresponding power spectra.

accelerations become significantly larger in the normal direction and again the low frequency modes do not seem to couple between the normal and tangential directions. The frequency spectra are significantly broader than in the previous regime, including frequencies (428 Hz) close to the first mode of beam 1 (457 Hz).

These vibrations continued for 3 h in a very periodic manner after which the test was stopped. A metallographic photo after 8 total hours of sliding is shown in Figure 3(c). Severe wear is apparent, as is local melting of certain spots on asperities. The in-plane dimensions of the asperities do not change much from the previous regime but a finer structure of the surface is nonetheless to be noted.

In what follows, attention will be focused on the low frequency vibration regime where all data signals are most reliable. Obviously, the duration of each regime depends on the combination of control parameters chosen. The most important trends to be noted are that the duration of the first sliding regime decreases with increasing normal force, frequency and amplitude, the rate of wear being increased in such situations. However, for the parameter combinations studied, the duration of this low frequency regime is at least five times the duration of the periodicity tests reported below.

3.2. STICK RELATED TRANSIENTS

Returning to the asymmetries observed in the low frequency vibration regime, the effects of slip reversal on the friction force are examined in more detail. Several tests were conducted for two beam stiffnesses k (1245 and 8446 N/m), varying separately the normal force ($t_N \in [0, 40$ N]), the forcing frequency ($f \in [3, 10$ Hz]) and the forcing amplitude ($A \in [0, 6{\cdot}3$ mm]). The nature of the into and out of stick transients was investigated as the control parameters were varied, as discussed below.

3.2.1. *Forcing frequency variation*

In the tests presented, $t_N = 5{\cdot}6$ N and $A = 2$ mm, while f was varied. First, some results for $k = 1245$ N/m are presented. For $f = 7{\cdot}0$ Hz (close to the natural frequency of the beam), the slider sticks at all times to the friction plate (Figure 6(b)) such there is no phase lag between the stage and slider displacements. This occurs because close to resonance (7·9 Hz) the force required to deflect the beam is comparatively small. Interestingly, at lower frequencies the slider displacement peaks lead the stage displacement peaks (negative phase lag—Figure 6(a)) while at higher frequencies slider displacement peaks lag the stage displacement peaks (positive phase lag—Figure 6(c)). In a particular test the phase lag can

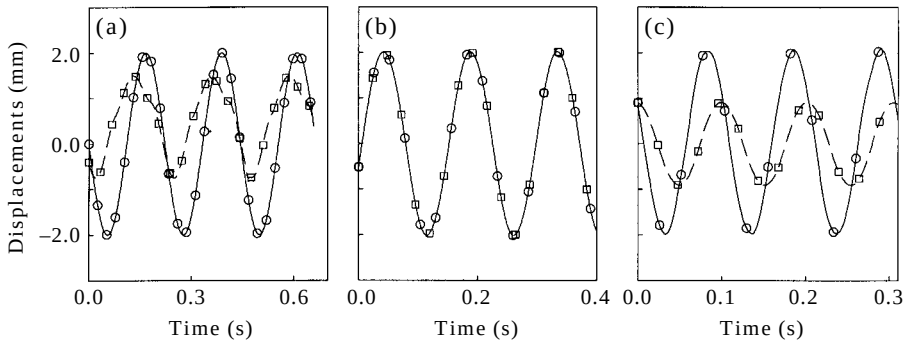

Figure 6. Illustration of the phase lag for the case of $t_N = 5{\cdot}6$ N and $A = 2$ mm: (a) mass displacement peaks (□) lead stage displacement (○) ($f = 4{\cdot}5$ Hz); (b) mass displacement peaks coincide with stage displacement peaks ($f = 7{\cdot}0$ Hz); (c) mass displacement peaks lag stage displacement peaks ($f = 10{\cdot}0$ Hz).

be calculated as the time shift at which the cross-correlation between the stage and slider displacements is maximum. In the results that follow, this phase lag is non-dimensionalized by multiplying it with the natural frequency.

Figure 7(a) presents the variation of the non-dimensional phase lag with f. When the forcing frequency is increased (circles), the phase lag is negative until $f = 7{\cdot}0$ Hz, when stick at all times occurs. Complete stick persists until $f = 9{\cdot}1$ Hz, after which relative sliding occurs with a positive phase lag. Upon decreasing f from 10 to 3 Hz (squares), the phase lag shows an obvious hysteretic effect suggestive of path-dependent behaviour. A loop described by t_T/t_N as a function of the relative velocity is shown to collapse to a flat zero relative velocity segment (Figure 7(b)) for $f = 8{\cdot}0$ Hz, when permanent stick occurs. Further, the time series in Figure 7(c)–(e) suggest that system response is markedly different at low frequencies than at higher ones. For $f = 3$ Hz, t_T/t_N exhibits several spikes associated with rapidly varying relative velocity (multiperiod motion). For 6 and 10 Hz, the relative velocity is much closer to a sinusoid, t_T/t_N showing distinct peaks upon slip direction reversal. In all cases sharp peaks of t_T/t_N are associated with rapid changes in sliding velocity, in a manner consistent with observations in reference [12] made for much smaller relative velocities.

3.2.2. *Normal force influence*

Several tests were run in which normal force was varied while the forcing frequency and amplitude were held constant. Here results are presented for $f = 3$ Hz and $A = 2$ mm.

Figure 8(a) indicates again a hysteretic effect as normal force is varied. The fact that complete stick behaviour occurs at different values of normal force upon loading and unloading suggests that the so called static coefficient of friction is at least a weak function of the normal force history. The maximum apparent coefficient of friction is a generally decreasing function of the normal load as can be seen in Figure 8(b), with a slight increase in μ_{max} to be noted during the unloading branch. The trajectories described by plots of t_T/t_N versus relative velocity are quite intricate, as depicted in Figures 8(c) and (d). For both cases shown, clockwise and counter-clockwise loops are noted in the same test, which is to our knowledge an unprecedented observation.

Time series for t_T/t_N and relative velocity are shown in Figure 9 for the normal forces marked in Figure 8(a). For lower normal forces (Figure 9(a) and (f)) several spikes are clearly seen in the evolution of t_T/t_N, corresponding as before to rapid changes in relative velocity at slip direction reversal. As t_N increases (7·8 N), the spikes decrease in magnitude, as does the amplitude of the relative velocity. Further increase of the normal force (Figures 9(c) and (d)) leads to further decrease of the relative velocity and smoother evolution of the apparent coefficient of friction. At 21·2 N (Figure 9(c)), stick occurs at all times and the relative velocity becomes zero at all times while the variation of t_T/t_N is very smooth and follows the displacement of the stage.

Other experiments show that at higher frequencies, the phase lag becomes positive while the hysteresis-like effect is more pronounced. It can be generally inferred that over the investigated range of the normal force the maximum of t_T/t_N decreases with increasing normal force, while the apparent coefficient of friction evolves more smoothly for higher normal forces.

3.2.3. *Forcing amplitude variation*

Fixing this time the normal force (5·6 N) and the forcing frequency, the forcing amplitude was varied in a series of experiments. First, the case where $k = 1245$ N/m and $f = 5$ Hz (Figure 10) is considered. At low forcing amplitudes (up to $A = 1{\cdot}05$ mm) the slider sticks at all times to the friction plate (Figures 10(a) and (b)). An increase of 0·05 mm

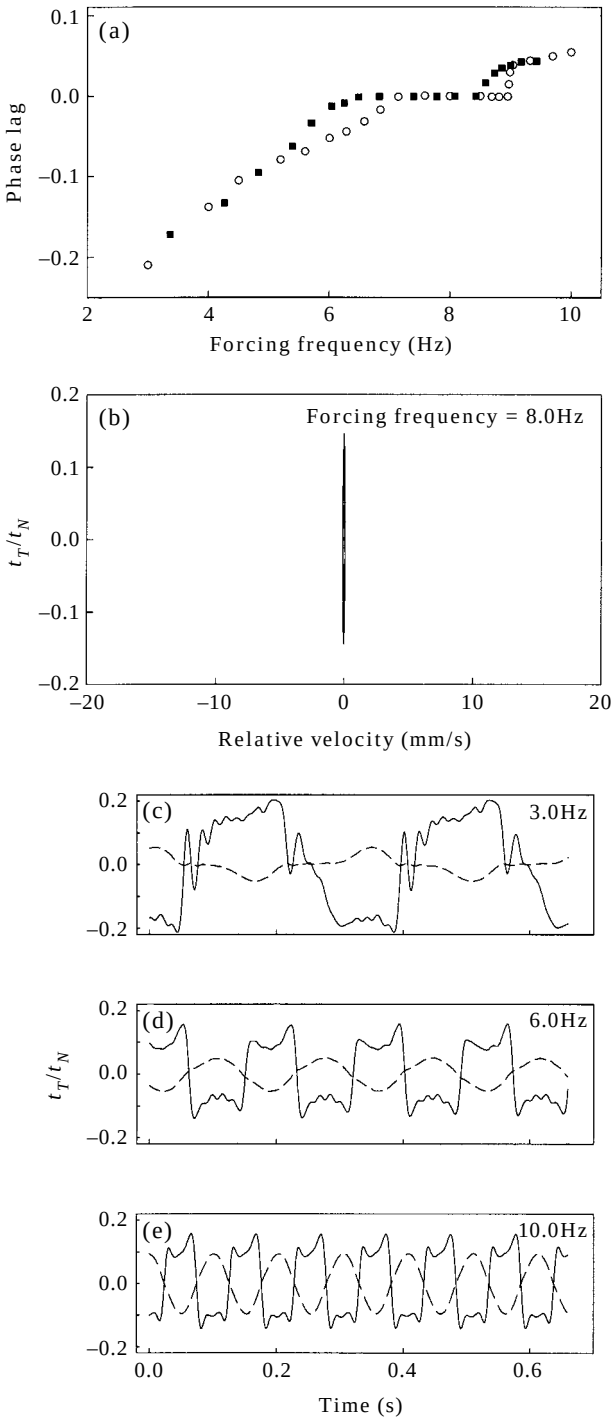

Figure 7. (a) Monitoring of phase lag versus forcing frequency reveals a notable hysteretic effect between the increasing and decreasing branches (○, increasing frequency; ■, decreasing frequency); (b) variation of the apparent coefficient of friction versus relative velocity for a forcing frequency where permanent stick occurs (8·0 Hz); (c), (d) and (e) typical evolutions of the apparent coefficient of friction (solid line) for forcing frequencies 3·0 Hz (c), 6·0 Hz (d), 10·0 Hz (e). The dashed line is the relative velocity (m/s). $A = 2$ mm, $t_N = 5{\cdot}6$ N and $k = 1245$ N/m.

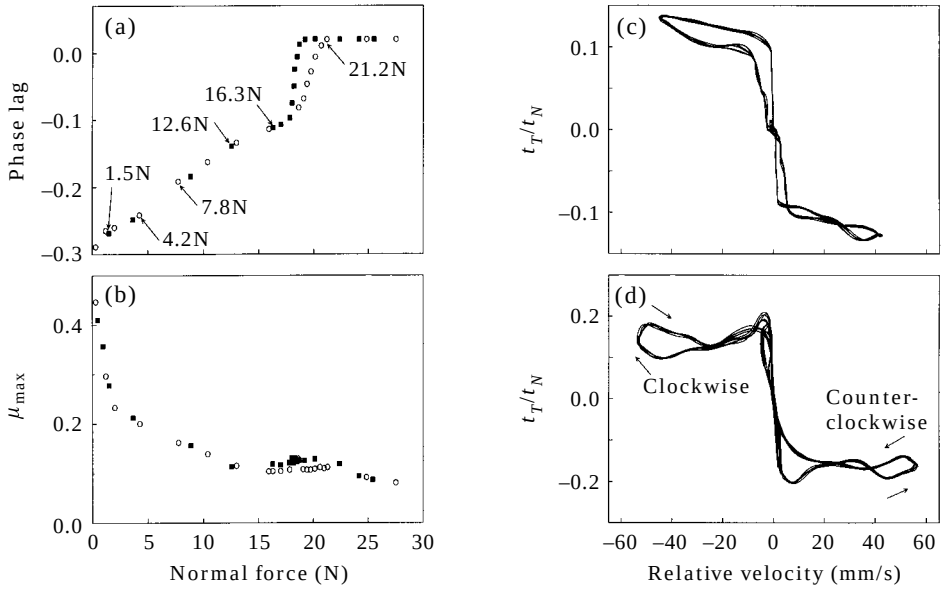

Figure 8. (a) Variation of the phase lag as normal pressure is varied, displaying again path dependence; (b) maximum apparent coefficient of friction as a function of the normal load; (c) and (d) loops described by the apparent coefficient of friction for two different normal loads, with both clockwise and counter-clockwise loops observed in the same experiment. $f = 3$ Hz, $A = 2$ mm and $k = 1245$ N/m. In (a) and (b): ○, loading; ■, unloading. In (c), normal load = 7·8 N; in (d), normal load = 4·2 N.

in forcing amplitude ($A = 1{\cdot}10$ mm) leads to a sudden large macro slip response as seen in Figure 10(c). Further increase in amplitude leads to higher relative velocities. For $A = 2{\cdot}09$ mm, t_T/t_N displays very sharp peaks at slip reversal. Further increase in forcing amplitude leads to maximum relative velocities higher than 100 mm/s and the average

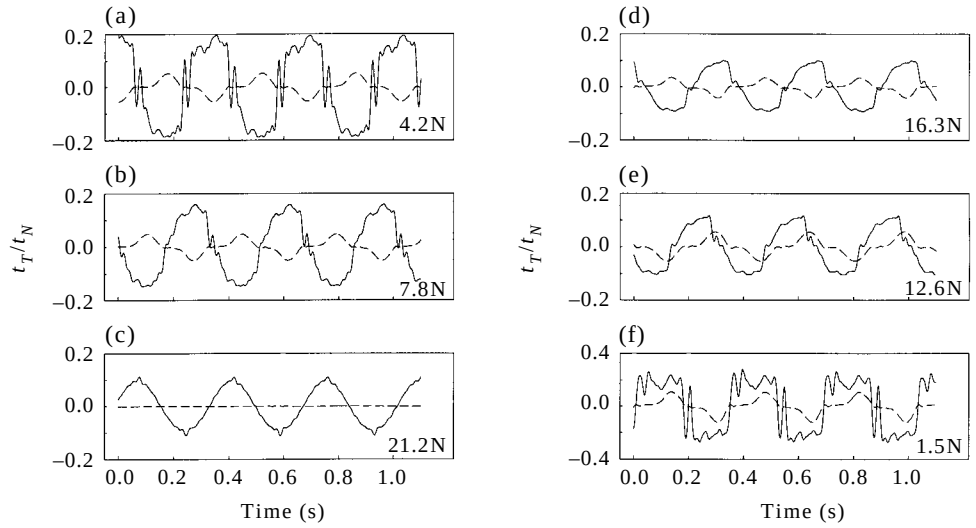

Figure 9. Typical evolutions of the apparent coefficient of friction (solid line) for normal forces (a) 4·2 N, (b)7·8 N, (c) 21·2 N, (d) 16·3 N, (e) 12·6 N, (f) 1·5 N. The dashed line is the relative velocity (m/s). (a), (b) and (c) loading branch; (d), (e) and (f) unloading branch. $f = 3$ Hz, $A = 2$ mm and $k = 1245$ N/m.

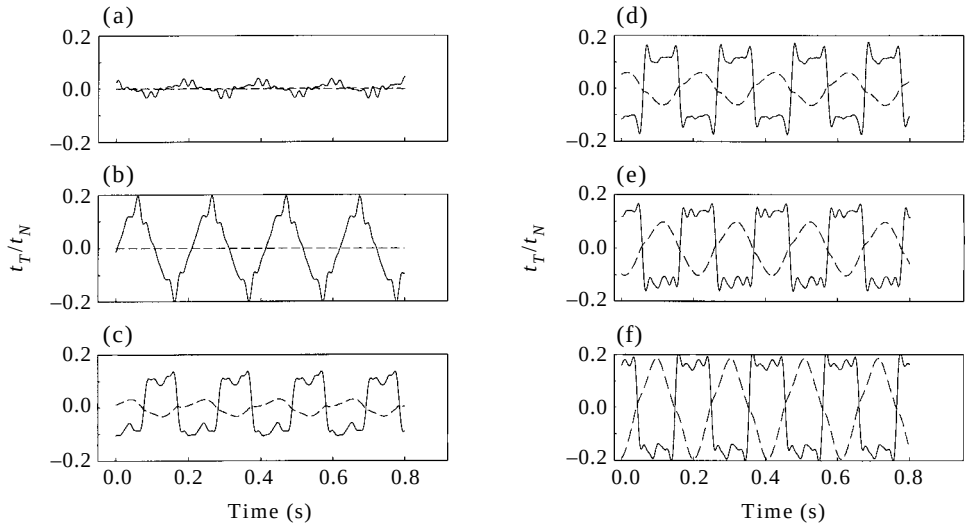

Figure 10. Typical evolutions of the apparent coefficient of friction (solid line) for different forcing amplitudes. The dashed line is the relative velocity (m/s). $f = 5$ Hz, $t_N = 5{\cdot}6$ N and $k = 1245$ N/m. (a) $A = 0{\cdot}18$ mm, (b) 1·05 mm, (c) 1·10 mm, (d) 2·09 mm, (e) 3·28 mm, (f) 6·21 mm.

value of t_T/t_N increases slightly (Figures 10(e) and (f)) while the peaks at slip reversal are not as pronounced for these higher velocities.

The observations of this section can be summarized as follows: (1) No significant variations of normal force and normal acceleration were seen in these experiments. Thus, the influence of the normal degree of freedom on all trends observed is believed to be minimal. (2) The evolution of t_T/t_N is potentially quite intricate in a given experiment, with its qualitative nature depending on all control parameters t_N, f, A and k. For certain choices of these parameters the apparent coefficient of friction evolved in both clockwise and counter-clockwise loops when plotted versus the relative slip velocity. (3) In monitoring the phase lag between the stage and slider displacements, variation of various control parameters (most notably normal force and forcing frequency) produced hysteretic behaviour, manifested as observed earlier as asymmetries in the associated stick–slip motions. (4) Increasing normal force has been seen to have two effects: (1) decreasing of the maximum apparent coefficient of friction (in accordance with many experimental observations, e.g., reference [14]); and (2) smoothing of t_T/t_N evolution, lowering the influence of relative sliding velocity in a manner consistent with the results of Kragelskii [15].

3.3. PHASE PORTRAITS AND ROUTES TO CHAOS

All four control parameters (k, f, A and t_N) were systematically varied over the ranges of interest to study trends in system periodicity. The configuration of the experimental set-up allowed for more refined variation of the forcing amplitude than of other system parameters, such that most of the tests considered variations of this parameter. Using $k = 8446$ N/m, $t_N = 6{\cdot}2$ N, and three different forcing frequencies, the forcing amplitude was continuously and very slowly (≈ 4 μm/s) increased while periodically sampling the slider trajectories. If an initially steady state is reached, then such slow sweeps in amplitude should introduce only negligible transients [16]. The resulting slow sweeps shown in Figure 11 show dramatically different bifurcation patterns depending on forcing frequency. All sweeps possess a zero relative velocity portion at low amplitudes after which bifurcations patterns are seen to strongly depend on f.

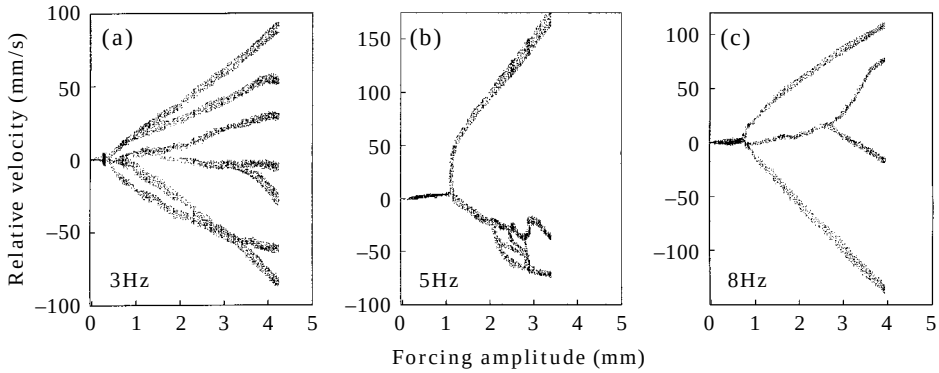

Figure 11. Bifurcations in the periodicity of the slider as the forcing amplitude is slowly varied: $t_N = 6{\cdot}2$ N, $k = 8446$ N/m. (a) $f = 3$ Hz, (b) $f = 5$ Hz, (c) $f = 8$ Hz.

For $f = 3$ Hz, a very narrow chaotic window is encountered immediately after the zero relative velocity portion with a typical irregular trajectory shown in Figure 12(a) for $A = 0{\cdot}4$ mm. The Poincaré section (sampling performed once per forcing cylce) in Figure 12(b) has a zero relative (stick) portion and two unsymmetric branches, suggesting a chaotic motion. The map has two cusp-like points, with precise identification of the slipping and sticking portions of the Poincaré section being difficult due to imprecisions

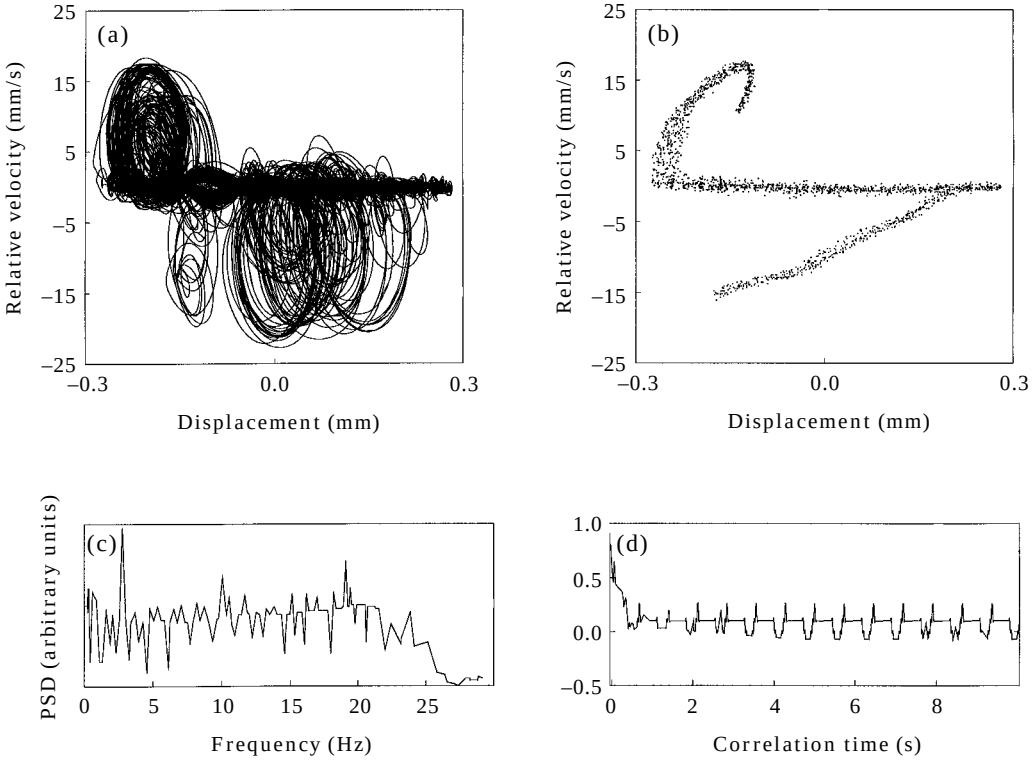

Figure 12. (a) For a small variation in the forcing amplitude, the slider enters a chaotic regime (500 forcing cycles are plotted), $A = 0{\cdot}40$ mm; (b) Poincaré sampling of the trajectories in (a); (c) frequency spectrum and (d) autocorrelation of the trajectories in (a); $t_N = 6{\cdot}2$ N, $f = 3$ Hz, $k = 8446$ N/m.

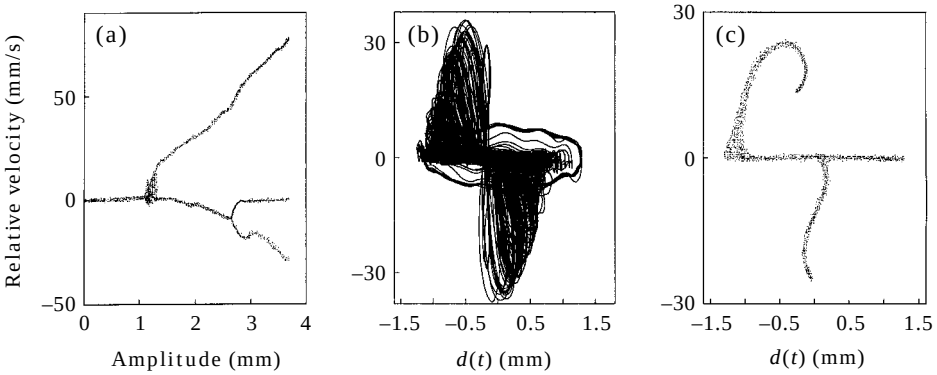

Figure 13. (a) Bifurcation patterns for a slow variation of the forcing amplitude; the transition from one period permanent stick motion occurs through a very narrow chaotic window; (b) chaotic trajectory of the slider ($A = 1{\cdot}27$ mm); (c) Poincaré section of the trajectories in (b); $f = 3$ Hz, $k = 1547$ N/m, $t_N = 6{\cdot}3$ N.

in calculating relative velocities. Broad band response in the frequency spectrum (Figure 12(c)) and rapid tendency of the autocorrelation to zero (Figure 12(d)) provide further evidence for the appearance of chaos in this experiment.

For a lower stiffness ($k = 1547$ N/m), an amplitude sweep (Figure 13(a)) shows even fewer bifurcations then before. This time a fuzzy transition from permanent stick (at lower amplitudes) to multiperiod motion suggests the presence of a chaotic window. Indeed, the phase portrait in Figure 13(b) suggests an irregular motion while the Poincaré section in Figure 13(c) suggests again a one-dimensional attractor. Qualitatively, the section is similar to the one in Figure 12(b) although the cusp-like features are not present anymore and one of the non-zero relative velocity branches starts from the middle of the stick portion. As amplitude is further increased the motion becomes periodic while the low velocity/stick portion of the protrait shrinks.

Moreover, for the softest beam tested ($k = 410$ N/m), no bifurcation occurs as will be shown later in Figure 19(c).

The observations in this section might be summarized as follows: (1) As the stiffness of the main beam increases, the system exhibits increasingly richer multiperiod motion, with bifurcations in slow sweeps being a more prominent feature as stiffness is increased. At lower k less force is required to deflect the beam, making the slider more likely to follow the period-one motion of the stage. (2) In relative velocity-slider displacement co-ordinates, the appearance of a typical phase portrait seems to include a zero (stick)/low velocity portion and a number of loops at higher relative velocities, with the number of the loops depending strongly on all control parameters. (3) Chaotic motion was always found to occur at the transition between permanent stick motion and multiperiod response, and was always confined to a very narrow window of the control parameter. These chaotic motions consist of irregularly alternating stick and slip periods, with the transients between phases occurring in an unpredictable manner. The attractor seems to be one-dimensional and qualitatively similar for various combinations of the control parameters.

4. NUMERICAL MODELLING

Modelling frictional oscillators with a great deal of generality is difficult because the physics of dry friction are not completely understood. Some of the frictional effects expected to be present in certain circumstances include velocity weakening dependencies

(e.g., reference [9]) and coupling between normal microvibrations and tangential slip instabilities [17]. In the current study, however, our experiments have shown the influence of the normal degree of freedom on system response to be minimal. The experimental results have also demonstrated that the velocity dependencies are an important factor in system dynamics, as are hysteretic effects (i.e., path dependence) in some circumstances. Accordingly, in our numerical efforts here a rate- and state-dependent frictional model is considered that has been described in detail elsewhere [11]. First, its characteristics are summarized, and then its predictions of system response are presented for the experimental system described in this paper.

4.1. RATE- AND STATE-DEPENDENT FRICTION

Observed rate and history effects are just two examples of behaviours which Coulomb models have difficulty predicting. Accordingly, several authors (e.g., Dieterich [18], Ruina [12], Rice and Ruina [19]) have considered the so-called state variable approach to friction modelling, whereby the condition of an interface at any instant is characterized by a set of (state) variables that tend to steady state values as constant velocity sliding occurs for a sufficiently long time. Changes in velocity produce evolution of these variables, contributing to a transient response with fading memory of prior slip history.

The particular state variable model utilized was originally developed for large deformation finite element applications involving interfacial rate dependence and associated instabilities [11]. Here it is described in a one-dimensional context so that its general properties can be understood. Formally, a slip function Φ is defined such that the dependence of the frictional traction t_T on a single state variable α is included:

$$\Phi := |t_T| - t_N(\mu + K_1(\alpha)), \qquad K_1(\alpha) = C_1(e^{\alpha/r} - 1), \tag{1}$$

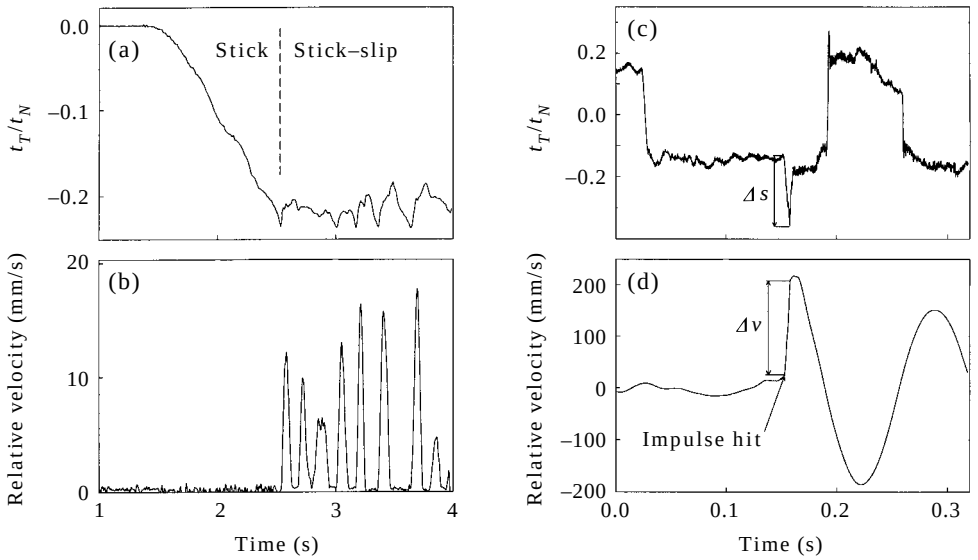

Figure 14. (a) and (b) Estimation of the static coefficient of friction (μ) from a constant velocity (4·1 mm/s) pulling test. Stick–slip oscillations are seen to occur; from the value of the ratio t_T/t_N at the end of a stick phase immediately prior to a slip phase one can estimate μ. (c) and (d) Estimation of the fluidity parameter η: (c) t_T/t_N is seen to increase sharply when a sharp velocity increase is imposed, (d) by impulse hitting the slider and keeping t_N constant; $k = 1140$ N/m, $t_N = 4{\cdot}8$ N.

where t_N is the normal pressure, K_1 is a user specified function, μ is the static coefficient of friction, and α, r and C_1 are model parameters (see reference [11]). Analogous to the situation with a yield function in plasticity, Φ is less than zero when frictional stick occurs and is either zero or positive (in the case of viscoplastic loading) otherwise; consideration of Φ thus amounts to establishing a slip criterion for frictional response.

The aforementioned fading memory is effective over a critical sliding distance D_c related to the average asperity spacing, and is assumed to be independent of the sliding velocity. The evolution law for α takes the form

$$\dot{\alpha} = -\frac{|V|}{D_c}[\alpha + C_2(|V|)], \tag{2}$$

where the constant $C_2 > 0$ is taken as the reciprocal of a characteristic velocity, and V is the relative sliding velocity. Evolution of α and its presence in the slip function (1) facilitates description of the desired history dependence.

Finally, it is usually observed that although the steady state coefficient of friction decreases with increasing slip velocity, rapid slip rate increases (decreases) generally produced strengthening (weakening) behaviour. Such a response might be expected as a result of the viscoplastic shearing of asperities. Accordingly, a viscoplastic regularization [13] is introduced into the constitutive model, providing a linear viscosity η to describe such effects:

$$V = \frac{1}{\eta}\left\langle \frac{\Phi}{t_N} \right\rangle, \tag{3}$$

where $\langle \cdot \rangle$ represents the MacAuley bracket function (0 if the argument is negative and equal to the argument for a positive operand).

Collection of the three main model components expressed by equations (1)–(3) renders the following constitutive model:

$$\Phi := |t_T| - t_N(\mu + K_1(\alpha)), \qquad \dot{t}_T = \varepsilon_T\left[V - \frac{1}{\eta}\left\langle \frac{\Phi}{t_N} \right\rangle \operatorname{sign}(t_T)\right],$$

$$\dot{\alpha} = -\frac{1}{D_c \eta}\left\langle \frac{\Phi}{t_N} \right\rangle\left[\alpha + C_2\left(\frac{\langle \Phi \rangle}{t_N \eta}\right)\right], \tag{4}$$

where the elastic stiffness ε_T has been introduced to allow for reversibly compliant behaviour before the onset of slip. In the event that rigidly perfect stick is desired this parameter can be set as large as practical so that only negligible pre-slip tangential motion occurs.

The behaviour of this model in two specialized instances provides insight into its various constituents. First, if constant velocity sliding has occurred for some time (steady state conditions), then $\dot{\alpha} = 0$ and

$$\left[\frac{|t_T|}{t_N}\right]_{ss} = \mu + K_1(-C_2(|V|_{ss})) + \eta|V|_{ss}. \tag{5}$$

This fact gives a practical method for prescription of the function K_1: it can be selected to give the best representation of measured apparent coefficient of friction $|t_T|/t_N$ versus sliding velocity $|V|$ under steady state conditions. Second, one also finds that an

instantaneous change in velocity leaves α with no opportunity to evolve, producing the following change in frictional stress:

$$\frac{|t_T^+| - |t_T^-|}{t_N} = \eta[|v^+| - |v^-|], \tag{6}$$

where $-$ and $+$ indicate values immediately before and after the imposed jump. This is a particular example of the viscous response discussed earlier.

Several comparisons of this model's predictions with varied experimental data are reported in reference [11], with success to be noted in large deformation metal forming problems, prediction of stable slip limits, and representation of an intricate response to elaborate slip histories. In the following, its capacity to reproduce the behaviours observed in this set of experiments is explored.

4.2. ESTIMATION OF MODEL CONSTANTS

In the current investigation, several tests to determine the model parameters were conducted, with particular emphasis on the static coefficient of friction μ and the fluidity parameter η. In Figure 14, the results of two such tests are presented. Figures 14(a) and (b) show the results obtained by pulling the stage at a constant velocity with an essentially inextensible string, with the initial peak in friction force giving the static coefficient of friction value. Repetition of such tests for various normal pressures ($t_N \in [3 \cdots 10]$ N) and pulling rates produced values of μ ranging between 0·21 and 0·26.

The experimental results in Figure 14(c) and (d), on the other hand, strongly suggest the presence of viscous effects, and provide also a technique for measuring the viscosity η. The stage was set in harmonic motion with $A = 2$ mm and $f = 3$ Hz to establish a relative motion between the slider and the stage, after which the slider was hit impulsively. Using the slip rate change Δv and the induced jump in the apparent coefficient of friction Δs, η may be estimated simply via

$$\eta = \frac{1}{\Delta v} \cdot \Delta s. \tag{7}$$

Various tests were run for different values of normal pressure and impulse levels, with the calculated fluidity parameter varying quite widely between 0·3 and 1·2 s/m.

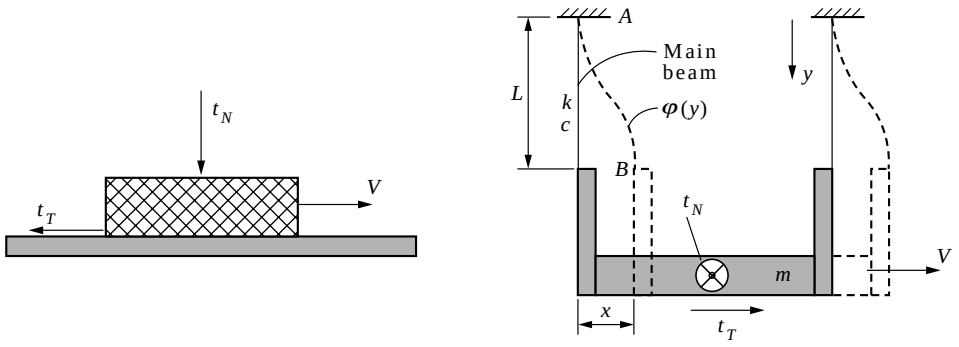

Figure 15. Schematic representation of the models used in the numerical simulations: (a) simple block driven with prescribed motion V as obtained from experiment; (b) spring–mass system for simulating the dynamics of the whole system.

With these tests as background, the model parameters used in the simulations that follow were: $C_1 = \mu$, $r = 1$, $\mu = 0{\cdot}25$, $\eta = 0{\cdot}3$–$1{\cdot}2$ s/m, and $D_c = 15$–25 μm (the latter values being chosen according to the asperity sizes taken from Figure 3). The remaining parameter, C_2, was taken as the inverse of a characteristic velocity, chosen as the maximum relative velocity achieved in the experiment of interest.

4.3. NUMERICAL EXAMPLES

Two different numerical models were considered in the results that follow, as depicted schematically in Figure 15. The case in Figure 15(a) represents a model whereby a measured slip trajectory is given as input, and the predicted frictional traction history is compared to that observed in the experiment, facilitating assessment of the friction law independent of the dynamics of the system in which the interface is embedded. Such model predictions were obtained by numerical integration of equation (4) using a return map strategy analogous to thos incorporated in computational plasticity.

In the second model type (Figure 15(b)), the dynamics of the entire system are taken into account, taking the variables f, A, m, t_N, k, as input data and subsequently comparing the prediction to experiment. Assuming cosine mode shapes for the deflected beam and using Hamilton's principle [20] one easily obtains the mass of an equivalent one-dimensional oscillator,

$$m^*\ddot{x} + c\dot{x} + kx = t_T, \tag{8}$$

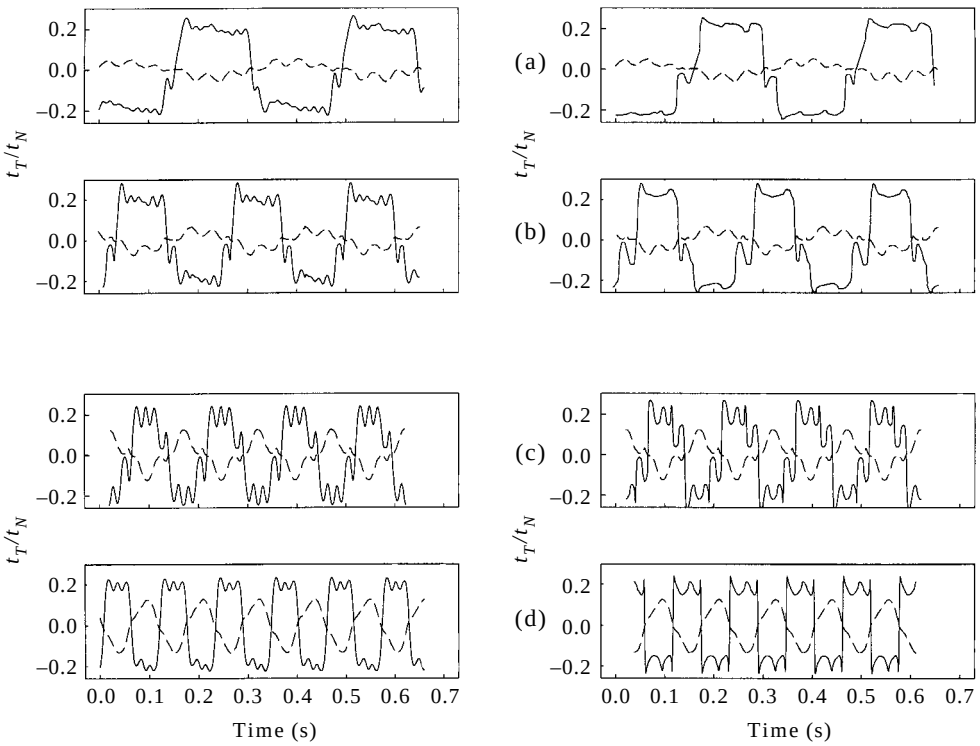

Figure 16. Using as input data a measured relative velocity trajectory, the integration of equation (4) yields corresponding model predictions of traction time history. Experimental data is in the left column and the corresponding numerical integrations are on the right. Model parameters: $\mu = 0{\cdot}25$, $\eta = 0{\cdot}8$ s/m, $D_c = 20$ μm $C_1 = 0{\cdot}25$, $r = 1$ and $C_2 = 0{\cdot}05$–$0{\cdot}12$ m/s. A simple Coulomb model would lead to a succession of step like traces. (a) 3·0 Hz, (b) 5·0 Hz, (c) 7·0 Hz, (d) 9·0 Hz.

with

$$m^* = \int_0^L m(y)\varphi(y)^2 \, \mathrm{d}y + m\varphi(L)_B, \tag{9}$$

where $m(y)$ is the distributed mass of the elastic beam per unit length, $\varphi(y)$ is the assumed mode shape and m the mass of the rigid head. The stiffness k and the damping c (very small) were measured directly, and in general varied from experiment to experiment. Response of this model was found by applying a variant of Newmark time integration to system (8).

4.3.1. *One-dimensional block driven with prescribed velocity*

First, the numerical model of the first type is considered (Figure 15(a)), using it to verify that representative frictional responses from our experiments could be reproduced. Figure 16 depicts the experimental and numerical results obtained for a particular combination of system parameters. This particular case corresponds to a combination of beam stiffness ($k = 8446$ N/m), forcing amplitude ($A = 2$ mm) and normal force ($t_N = 5{\cdot}6$ N) that produces slip behaviour throughout each cycle for all forcing frequencies studied. Acceptable agreement with experimental results is to be noted for all frequencies, with the response being characterized by a delicate interaction between softening state

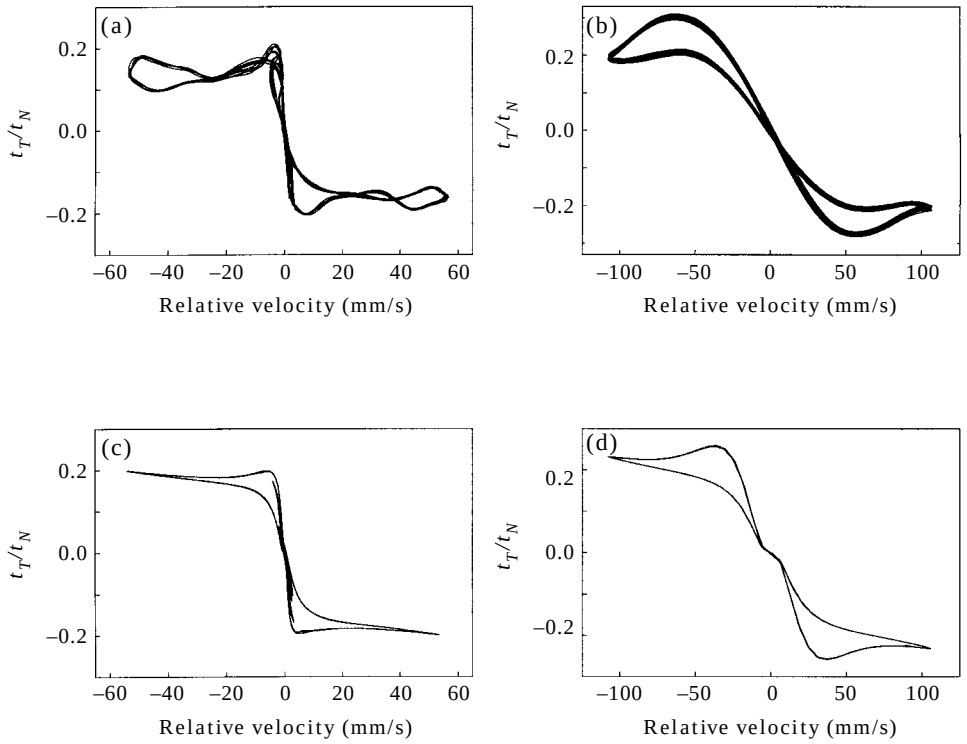

Figure 17. Clockwise loops described by the ratio t_T/t_N as a function of the relative velocity. As expected, counter-clockwise loops cannot be described. (a)–(b) Experimental result; (c)–(d) numerical simulations. (c) Model parameters: $\mu = 0{\cdot}25$, $\eta = 1{\cdot}1$ s/m, $D_c = 20$ μm, $C_1 = 0{\cdot}25$, $r = 1$ and $C_2 = 0{\cdot}05$ m/s, (d) model parameters: $\mu = 0{\cdot}25$, $\eta = 0{\cdot}7$ s/m, $D_c = 20$ μm, $C_1 = 0{\cdot}25$, $r = 1$ and $C_2 = 0{\cdot}1$ m/s. (a) and (c): Normal load = 4·2 N; (b) and (d): normal load = 0·9 N.

variable effects and strengthening viscous effects. In particular, the loops observed as t_T/t_N evolve in such experiments compare satisfactorily with data, as shown in Figure 17. However, the counter-clockwise evolutions observed in experiment cannot be predicted by the state variable model. This is the case because the model assumes that frictional force is an increasing function of recent slip, so that the apparent coefficient of friction must fall when the velocity (in absolute value) is decreasing (implying clockwise loops).

Examining now some experimental cases where stick may occur, the results of Figure 18 are presented, where the system parameters $k = 8446$ N/m, $f = 5$ Hz and $t_N = 8{\cdot}2$ N are held fixed while the forcing amplitude is varied. Wherever possible, the model of Figure 15(a) is still utilized, but for parameter combinations where stick appears in typical cycles the model of Figure 15(b) must be used (since for perfect stick the frictional traction is indeterminate for zero relative sliding velocity). Again, for the cases shown, good agreement with experimental results is to be noticed. Permanent stick occurs in

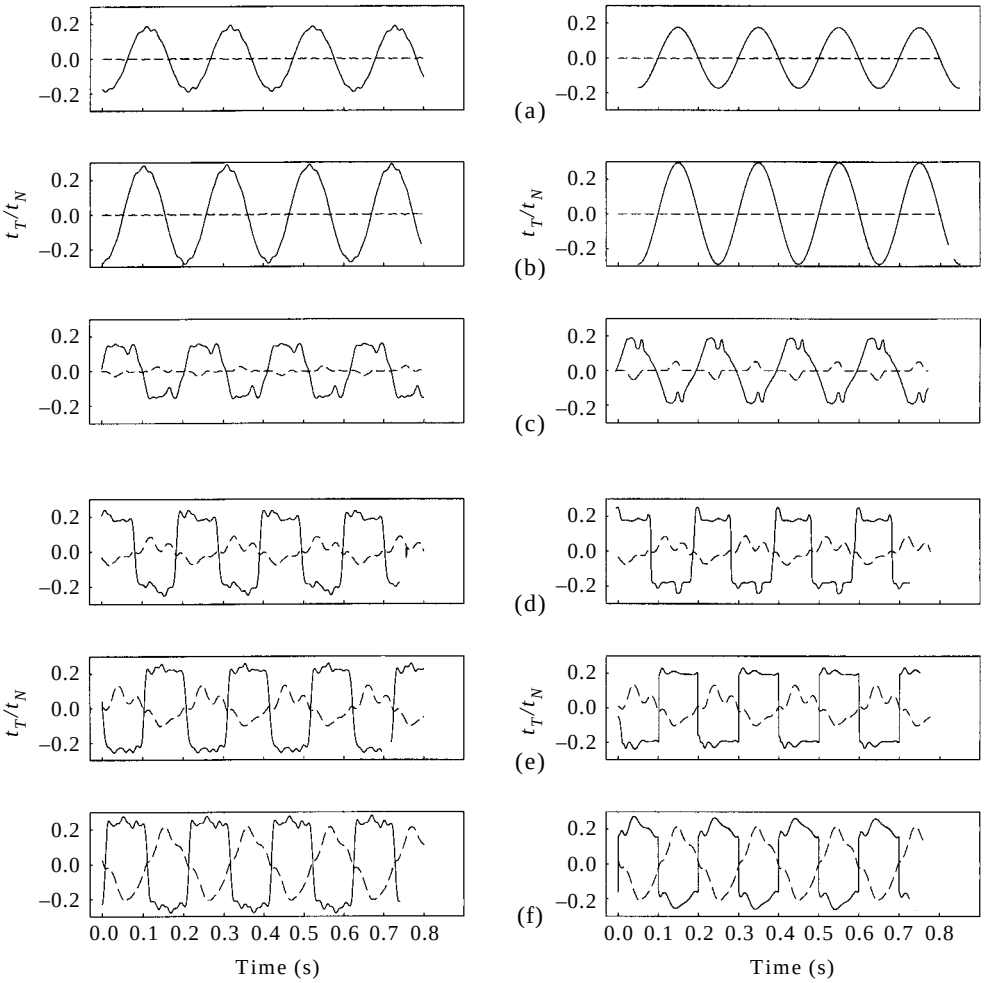

Figure 18. Model predictions for t_T/t_N using experimentally obtained velocity histories as input. Experimental data is in the left column and the corresponding numerical simulations are on the right. Model parameters: $\mu = 0{\cdot}25$, $\eta = 1{\cdot}0$ s/m, $D_c = 20$ μm, $C_1 = 0{\cdot}25$, $r = 1$ and $C_2 = 0{\cdot}05$–$0{\cdot}2$ m/s. (a) $A = 0{\cdot}19$ mm, (b) $0{\cdot}24$ mm, (c) $0{\cdot}31$ mm, (d) $1{\cdot}92$ mm, (e) $3{\cdot}12$ mm, (f) $6{\cdot}11$ mm.

Figure 18(a) and (b), with larger amplitude forcing producing some slip and an accompanying drop in maximum friction force.

In summarizing these predictions, it is emphasized that a simple Coulomb model will predict only step like evolutions of t_T/t_N in response to changes in sign of sliding velocity. One might conclude from these simulations that the state variable approach can be used to model friction force evolutions for a large variety of slip histories where Coulomb

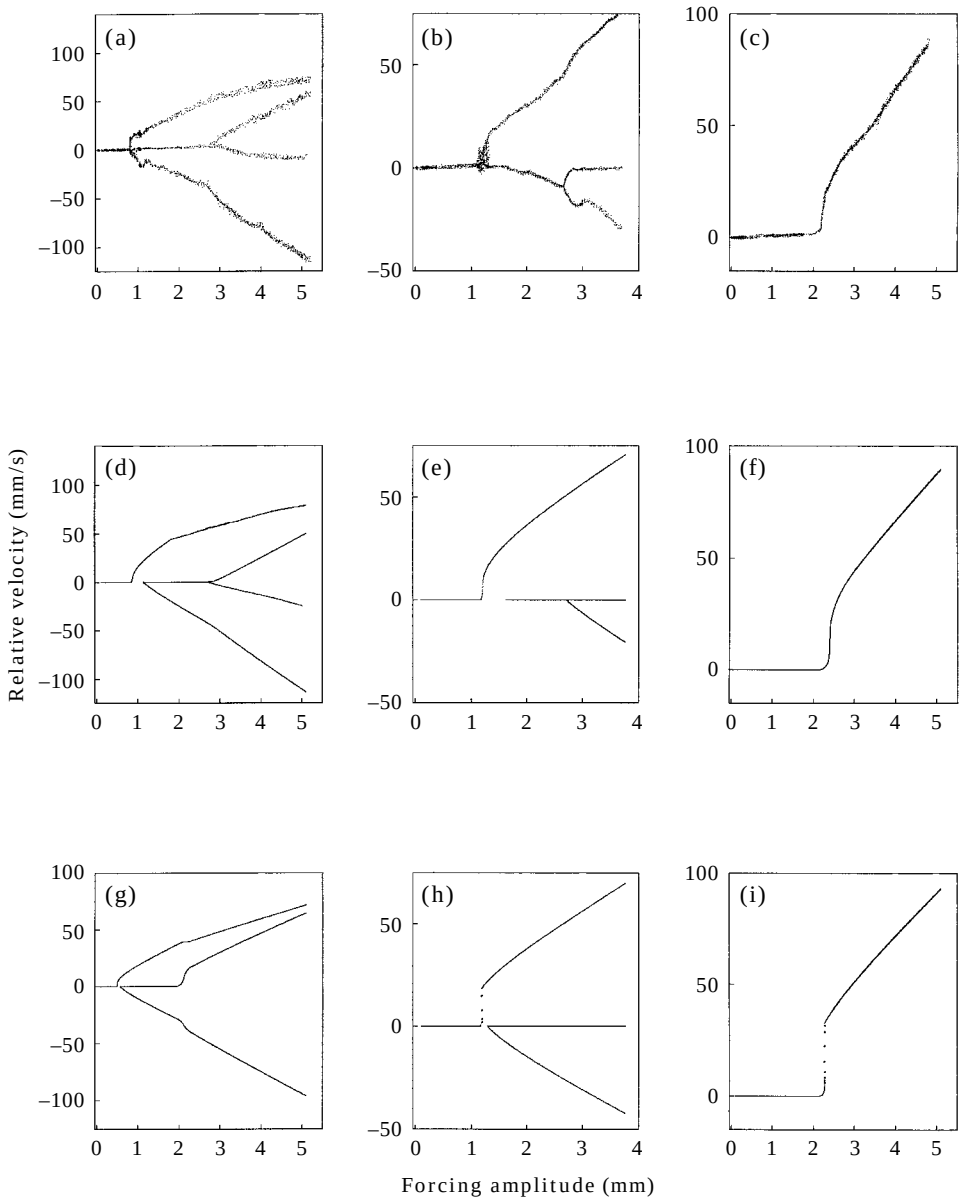

Figure 19. Numerically simulated evolution of bifurcation diagrams as the forcing amplitude A is slowly varied for three different stiffnesses for both the state variable (d)–(f) and the simple Coulomb model (g)–(i). Model parameters: $\mu = 0{\cdot}25$, $\eta = 0{\cdot}6$ s/m, $D_c = 20$ μm, $C_1 = 0{\cdot}25$, $r = 1$ and $C_2 = 0{\cdot}1$ m/s. Experimental bifurcation sequences (a)–(c); $f = 3$ Hz and $t_N = 6{\cdot}3$ N. (a, d, g) $k = 3034$ N/m; (b, c, h) $k = 1547$ N/m; (c, f, i) $k = 410$ N/m.

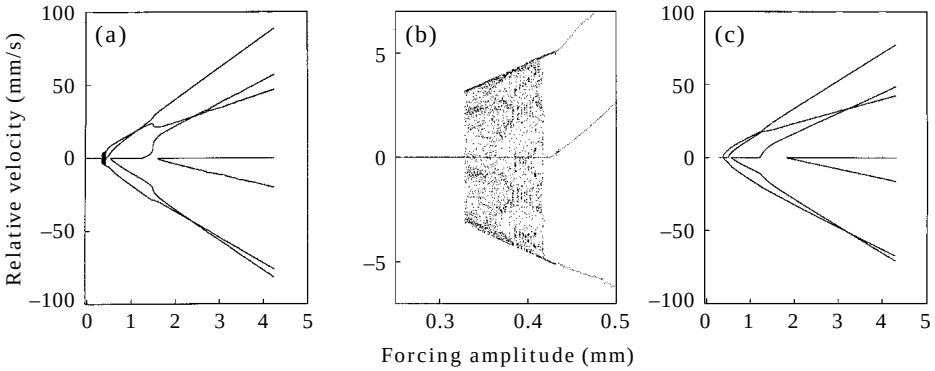

Figure 20. Calculated bifurcations in the periodicity of the slider as the forcing amplitude is slowly varied: $t_N = 6{\cdot}2$ N, $k = 8446$ N/m, $f = 3$ Hz; same model parameters as in Figure 19. (a) State variable model; (b) detail of the data in (a); (c) Coulomb model simulation $\mu = 0{\cdot}25$. To be compared with data in Figure 11(a).

predictions are less than adequate, and that the model parameters required can be reasonably obtained from experiment.

4.3.2. *Bifurcation diagrams and chaotic motion*

Turning attention now to the predicted and measured patterns of periodicity displayed by the system, Figure 19(a)–(c) presents simulated and measured system response to a slow sweep in forcing amplitude. Numerical results are given both for the state variable model (Figure 19(d)–(f)) and for a simple Coulomb (static coefficient of friction equals the kinetic one) description (Figure 19(g)–(i)). One may note that the state variable predictions are superior to the Coulomb predictions, with the latter missing entirely some of the bifurcations observed in experiment.

When a stiffness higher than any of those in Figure 19 is utilized, ($k = 8446$ N/m), the results depicted in Figure 20 are obtained. A qualitatively good agreement with experimental data in Figure 11(a) may be noted in the case of the state variable prediction. The Coulomb model, while providing a reasonable representation of the bifurcation sequence that was measured, does not predict any of the irregular motion that was observed in the experiment and which was predicted by the state variable approach. As shown in the detail of the bifurcation sequence in Figure 20(b), irregular motion is seen

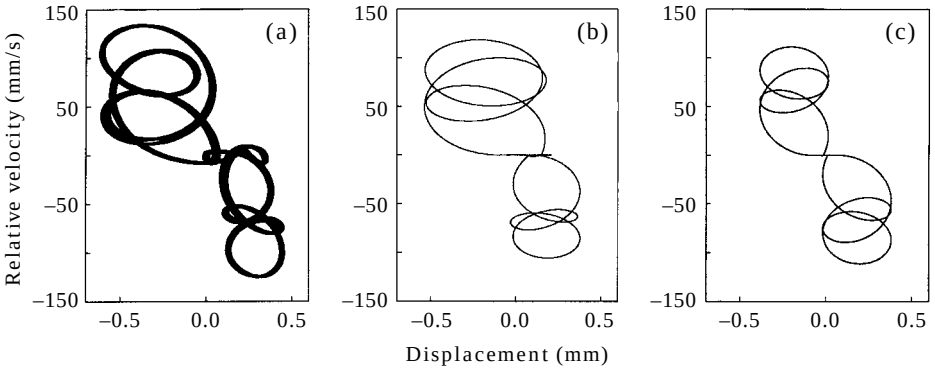

Figure 21. Periodicity in slider trajectories: (a) experimental; (b) state variable model; (c) Coulomb model. Control parameter values: $t_N = 6{\cdot}2$ N, $f = 3$ Hz, $k = 8446$ N/m, $A = 4{\cdot}62$ mm (500 cycles are plotted in each trajectory). Same model parameters as in Figure 19.

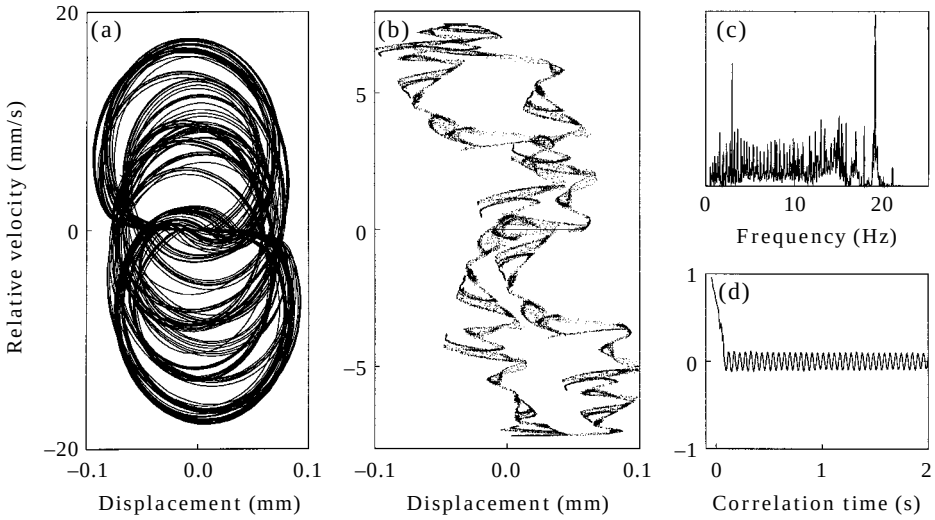

Figure 22. (a) Phase portrait for $A = 0{\cdot}40$ mm; (b) Poincaré section of the motion in (a) (40 000 points); (c) frequency spectrum (linear plot) and (d) autocorrelation of the motion in (a). Same parameters as in Figure 20.

to occur (for $A \in [0{\cdot}33 \cdots 0{\cdot}43]$mm) right after a permanent stick window for $A \leqslant 0{\cdot}33$ mm as was the case in the experiment.

Some numerically integrated phase portraits are shown alongside experimental counterparts in Figure 21. Again, results are shown for both state variable and Coulomb models for direct comparison, and suggest the superiority of the state variable model over the Coulomb prediction. In the cases where irregular response was predicted, numerical integrations produced phase portraits like those depicted in Figure 22(a). Both the Poincaré section in Figure 22(b) together with the frequency spectrum and autocorrelation in Figure 22(c) and (d) confirm that the motion is indeed chaotic. Although we were unable to closely replicate the observed strange attractor, the fact that irregular motion could be predicted where Coulomb models fail is an encouraging finding.

Finally, it is notable that the experiments conducted only exhibited chaotic behaviour at the transition from permanent stick motion to complex stick–slip behviour, and at small forcing amplitudes. For other types of interfaces it is speculated that chaotic motion may

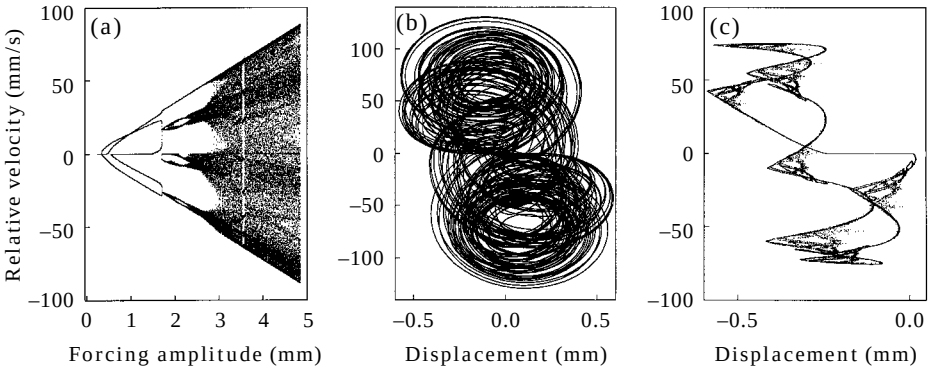

Figure 23. (a) Changing the interface fluidity parameter ($\eta = 0{\cdot}2$ s/m) and keeping all other parameters as in Figure 20, a significant change is produced in the bifurcation pattern, with irregular motion appearing also for larger A. (b) Phase portrait for an irregular motion ($A = 4$ mm); (c) Poincaré section of the motion in (b).

also occur at larger amplitudes. In support of this Figure 23 is presented where the fluidity parameter η was changed while holding all other parameters as before. It is clear from the figure that the bifurcation sequence in this case leads to chaotic behaviour for larger A.

5. SUMMARY AND CONCLUSIONS

This work has described experimental and numerical results for a simple friction oscillator excited harmonically through the frictional interface. Issues emphasized by the work include the effect of wear on the qualitative nature of stick–slip motion, the characterization of stick–slip related transients, and the non-linear dynamics of the frictionally damped system.

The important accomplishments of the experimental work are summarized as follows. (1) Identification of three distinct sliding regimes, qualitatively distinguishable by the amount of wear undergone and quantitatively characterized by the frequency content of the interface response. (2) Characterization of a ''smooth sliding'' regime, where the degree of wear remains modest and the higher system frequencies remain unexcited. No tangential–normal interfacial coupling was observed in this regime, and the low frequency nature of the interface response made it ideal for in-depth study. (3) Identification of complex trajectories of the apparent coefficient of friction during stick–slip, with both clockwise and counter-clockwise loops of this quantity being observed. Hysteretic effects were also prominent in parametric studies of stick–slip transients. (4) Measurement of the effect of control parameters on the evolution of periodicity and/or chaotic response in the system. Typical phase portraits included a zero/low relative velocity portion and a number of loops at higher relative velocity. The number of multiperiod harmonics increased with stiffness and excitation amplitude, and decreased for increasing interface pressure and forcing frequency. Chaotic motion was observed only at the transition between permanent stick motion and multiperiod response for the combinations of control parameters studied.

The modelling effort undertaken in support of these experiments produced much better agreement with experimental data than did a simple Coulomb model, both in predicting observed stick–slip time histories and in characterization of bifurcation sequences. These simulations featured a rate- and state-dependent friction model incorporating experimentally estimated model constants, suggesting that history and rate dependence can be realistically and simply incorporated into predictions where such effects are known to have important influence.

ACKNOWLEDGMENTS

The authors wish to thank Drs L. N. Virgin and J. F. Wilson of Duke University for their suggestions in various stages of this work. This effort was supported in part by the Mechanics and Materials Program of the National Science Foundation under Grant No. MSS-9308486; this support is gratefully acknowledged.

REFERENCES

1. R. Bell and M. Buderkin 1969 *Proceedings of the Institute of Mechanical Engineers* **184**, 543–560. A study of the stick–slip motion of machine tools feed drives.
2. U. Fingberg 1990 *Journal of Sound and Vibration* **143**, 365–377. A model of wheel–rail squealing noise.
3. G. H. M. Van der Heijden 1993 *Chaos*, *Solitons and Fractals* **3**, 219–247. Bifurcation and chaos in drillstring dynamics.

4. V. Aronov, A. F. D'Souza, S. Kalpajian and I. Shareed 1984 *Journal of Tribology* **106**, 54–58. Interactions among friction, wear and system stiffness—part 1: effect of normal load and system stiffness.
5. D. M. Tolstoi 1967 *Wear* **10**, 199–213. Significance of the normal degree of freedom and natural normal vibrations in contact friction.
6. A. Soom and C. Kim 1983 *Journal of Lubrication Technology* **105**, 221–229. Interactions between dynamic normal and frictional forces during unlubricated sliding.
7. D. P. Hess and A. Soom 1992 in *Fundamentals of Friction*: *Macroscopic and Microscopic Processes* (I. L. Singer and H. M. Pollock, editors) Boston: Kluwer Academic Publishers. Unsteady friction in the presence of vibrations.
8. J. Awrejcewicz 1986 *Journal of Sound and Vibration* **109**, 178–180. Chaos in simple mechanical systems with friction.
9. K. Popp and P. Stelter 1992 *Philosophical Transactions of the Royal Society of London*, *Series A* **332**, 89–105. Stick–slip vibrations and chaos.
10. B. Feeny and F. C. Moon 1994 *Journal of Sound and Vibration* **170**, 303–323. Chaos in a forced-friction oscillator: experiments and numerical modeling.
11. T. A. Laursen and V. G. Oancea 1997 *Computer Methods in Applied Mechanics and Engineering* **143**, 197–227. On the constitutive modeling and finite element computation of rate dependent frictional sliding in large deformations.
12. A. Ruina 1983 *Journal of Geophysical Research* **88**, 10359–10370. Slip instability and state variable friction laws.
13. P. Perzyna 1971 *Advances in Applied Mechanics* **11**, 313–354. Thermodynamic theory of viscoplasticity.
14. P. B. Madakson 1983 *Wear* **87**, 191–206. The frictional behaviour of materials.
15. I. V. Kragelskii 1965 *Friction and Wear* London: Butterworths.
16. L. N. Virgin 1986 *Journal of Sound and Vibration* **110**, 99–109. Parametric studies of the dynamic evolution through a fold.
17. J. T. Oden and J. A. C. Martins 1985 *Computer Methods in Applied Mechanics and Engineering* **52**, 527–634. Models and computational methods for dynamic friction phenomena.
18. J. H. Dieterich 1992 *Tectonophysics* **211**, 115–134. Earthquake nucleation on faults with rate and state dependent strength.
19. J. R. Rice and A. L. Ruina 1983 *Journal of Applied Mechanics* **50**, 343–349. Stability of steady frictional slipping.
20. R. W. Clough and J. Penzien 1982 *Dynamics of Structures* Singapore: McGraw-Hill.